Synthesis of low-cost hydrochar using agro-industrial residues for the removal of pharmaceutical drug chloroquine

Alexandre Amado de Moura[a,*], Henrique Straioto[a], Wardleison Moreira Martins[a], Thiago Peixoto de Araújo[b], Alexandre Diório[a], Rosângela Bergamasco[a], Murilo Pereira Moisés[c], Maria Angélica Simões Dornellas Barros[a]

[a]Department of Chemical Engineering, State University of Maringá, Colombo av. 5790, Building D-90, Maringá, PR, CEP 87020-900, Brazil, emails: eng.alexandre.amado@gmail.com (A.A. de Moura), henrique_72@hotmail.com (H. Straioto), wmmoreira@uem.br (W.M. Martins), adiorio2@uem.br (A. Diório), rbergamasco@uem.br (R. Bergamasco), masdbarros@uem.br (M.A.S.D. Barros)
[b]Federal University of Technology, Doutor Washington Subtil Chueire Street, 330, Ponta Grossa, PR, CEP, 84017-220, Brazil, email: thiago@flashrg.com.br (T.P. de Araújo)
[c]Federal University of Technology, Marcílio Dias Street, 635, Apucarana, PR, CEP 86812-460, Brazil, email: murilomoisesutfpr@gmail.com (M.P. Moisés)

ABSTRACT

The aim of this work was to synthesize a low-cost hydrochar via hydrothermal route using two residues from the sugar-energy industries: sugarcane bagasse and the high-pressure boiler water discharge. The applicability of the hydrochar in water treatment process was tested in the biosorption of chloroquine from water in a discontinuous process. The synthesized hydrochar exhibited a high specific surface area (~188 mg·g⁻¹) with average pore diameter <2.0 nm. The biosorption results showed a fast biosorption kinetic in the initial 10 min and an equilibrium time of ~60 min. Acidic properties of both contaminant and HC-T resulted in repulsive forces, therefore, basic conditions would represent the optimum condition for the highest chloroquine biosorption, but that is not interesting for a water treatment plant due to chemicals consumption for pH correction, costs and salinity problems. The pseudo-second-order kinetic and Sips isotherm models were the best models fitted to experimental data. The thermodynamic parameters indicated an endothermic and spontaneous biosorption. The maximum experimental biosorption capacity was 73.34 mg·g⁻¹ at 45°C. In conclusion, hydrothermal-activated carbon (HC-T) is a promising biosorbent, synthesized with an ecofriendly process, for the removal of chloroquine from contaminated waters due to the great availability, quantity and low-cost of sugarcane bagasse in the Brazilian territory, allied with the reusability of high-pressure boiler water.

Keywords: Biosorption; Hydrochar; Chloroquine; Covid-19; Agricultural residue

1. Introduction

The Covid-19 pandemic was one of the greatest challenges that the humankind faced in the 21st century. The virus spread rapidly around the world with a high infection rate and many deaths. In an attempt to stop or at least slow the infection and its symptoms, different therapeutic strategies and pharmaceutical drugs have been used such as antivirals, antibiotics, glucocorticoids and others, some of them even without a robust scientific background of its efficiency [1].

* Corresponding author.

The most famous and used pharmaceutical drug during the pandemic was chloroquine (CQ). Even though chloroquine is traditionally used to treat malaria infection [2], CQ was used by developing countries against Covid-19 as an alternative treatment to costly and/or unavailable antiviral drugs to treat the disease symptoms, for example, anti-inflammatory and antithrombotic effects. However, at high doses, CQ poses high toxicity that may lead to disabilities or even death [3].

The indiscriminate use of CQ or any other pharmaceutical drugs in general is of growing concern, since it is estimated that approximately 33% of the medicaments are excreted by the human body and end up being detected in hydric sources [4]. Conventional methods for water treatment are not efficient enough to completely remove or mineralize this class of emerging contaminants and, in this sense, additional polishing steps have been proposed and/or implemented for water treatment process intensification [5].

Several technologies are available for CQ removal such as biodegradation [6], Fenton oxidation [7] electro-Fenton oxidation [8], membrane process [9] and others [10] with unique advantages and drawbacks each one, but the biosorption technology [9] stands out in techno- and eco-centric features due to ease implementation and operation of reequipments, versatility towards different adsorbates and high removal efficiency [11]. Biosorption is the use of biomass to adsorb contaminants from an aqueous phase [12]. However, the choice of the biosorbent (biomass) is of huge importance for the success of the biosorption process in water treatment [13]. In this sense, it is desirable that the adsorbent promotes a rapid contaminant removal with a high biosorption/desorption capacity [14]. Thus, industrial and agricultural residues pose as the ideal candidates for adsorbent synthesis, such as the residues generated in the sugar-energy industries [15,16].

The sugar-energy industries generate a huge number and quantity of residues of heterogeneous characteristics and the sugarcane bagasse (SB) stands out with approximately 140 million ton generated every year in Brazil [17]. This residue is partially burned in furnaces for energy cogeneration and the remaining material is discharged. Therefore, a more noble destination for the residual SB is of interest such as the synthesis of a low-cost biosorbent [18]. Pyrolysis, hydrothermal carbonization (HC) and gasification are the most used thermochemical methods for turning SB into biosorbent [13]. For wet biomass, such as the SB, the HC method is often applied with the resulting material named hydrochar or biochar. HC conversion is conducted in a wet and pressurized furnace with temperatures ranging from 160°C–880°C for the oxidation of organic matter [13].

Another residue generated by sugar-energy industries is the water discharged by the high-pressure boiler (BD). In order to control the boiler pressure to optimal operational conditions, a discharge is continuously necessary, thus generating approximately 1.5 ton/h of liquid effluent that is sent to treatment ponds [8–9]. Due to the large amount of BD, it can be used in hydrothermal synthesis of new adsorbents from SB.

Therefore, the aim of this paper was to synthesize a hydrochar via hydrothermal route using two residues from the sugar-energy industries: sugarcane bagasse (SB) and the water discharged by the high-pressure boiler (BD). The applicability of hydrochar in water treatment processes was tested in the biosorption of the pharmaceutical drug chloroquine from synthetic contaminant water in a discontinuous process.

2. Materials and methods

2.1. Materials

Chloroquine diphosphate (95% purity) was purchased from a local drugstore (Farmácia Catanduvas, Brazil). The pharmaceutical drug was used in the biosorption experiments diluted in water with different concentrations and without any purification or pH adjustment (except when explicit mentioned). The stock solution of CQ was prepared by dissolving the contaminant in 1,000 mL of deionized water. The working solutions were prepared by diluting the stock solution with deionized water until the desired contaminant concentration.

The SB and the BD were provided from a Brazilian alcohol mill and were used in the hydrothermal conversion process. The BD was collected from the cogeneration boiler and stored in a freezer at –2°C until its use. The SB was also stored in a freezer at –2°C until being modified as hydrochar. Table 1 displays the characteristics of the CQ and BD used in this research.
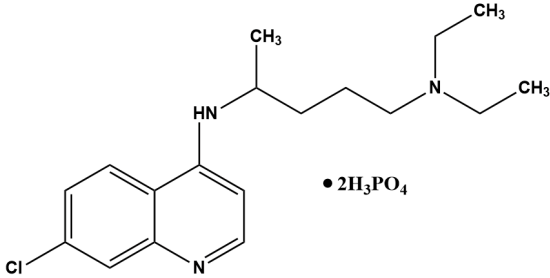
2.2. Sample characterizations

The SB and the synthesized low-cost adsorbent (hereafter named HC-T) were characterized. The materials morphology was characterized by means of a scanning electron microscopy (SEM; FEI-Quanta 250). The materials specific surface area (SBET) and volume of pores were determined by means of N_2-physisorption at 77 K (Micrometrics ASAP-2020) following to the BET protocol [20]. Elemental composition analysis was carried out to verify the carbon content the in a Perkin Elmer 2400 Series II CHNS/O with 1 mg sample at 1,000°C. Thermal stability was determined via thermogravimetric experiments (Perkin Elmer, STA) heating the samples until 900°C with a heating ramp of 10°C min⁻¹ and N_2-volumetric flow of 50 mL min⁻¹. The Fourier-transform infrared (FT-IR; Shimadzu IR Tracer-100) analysis in the range of 400–4,000 cm⁻¹ was used to identify surface modifications in the material due to the hydrothermal process. The adsorbent structure was characterized by X-ray diffraction (XRD; Shimadzu LabX 6000) with CuKα-radiation (λ = 0.154056 nm), 40 kV, 30 mA acquisition time of 1 s and rotational rate of 2θ min⁻¹ from 5° ≤ 2θ ≤ 85°. The charge distribution was analyzed by means of the pH of point of zero charge (pH_{PZC}) estimated by the "11-points protocol" [21].

2.3. Hydrothermal carbonization

Prior to the hydrothermal carbonization (HC) process, the SB was dried for 24 h at 100°C aiming to stop biological degradation undesired for the material. Then, the dry-SB was milled in a knife mill and sieved. The biomass that passed through the 20-mesh sieve was used in the hydrothermal carbonization process since it was the highest mass obtained.

Table 1
Physico-chemical properties for the CQ and BD

	Pharmaceutical contaminant	High-pressure boiler effluent	
Name	Chloroquine diphosphate	Property	Value
Molecular weight	515.86 g·mol^{-1}	pH	9.95
Molecular formula	$C_{18}H_{26}ClN_3 \cdot 2H_3PO_4$	Apparent color	Not color
Water solubility	20 mg·L^{-1}	Turbidity (NTU)	0.54
Maximum wavelength	λ_{max} = 343 nm	BOD (mg·L^{-1})	180.00
Molecular structure		COD (mg·L^{-1})	271.20
CAS number	50-63-5		
References	[19]		

The hydrochar (biosorbent) was synthesized using the dry-milled-sieved-SB and the hydrothermal carbonization process. To synthesize the biosorbent with the highest carbon content, a design of experiment was employed varying the SB-BD ratio, temperature and time of burning. Therefore, in this work, the low-cost biosorbent synthesized (named HC-T) used the following conditions: 1:3 (m/v) SB-BD ratio accommodated in a stainless-steal autoclave coated internally with Teflon®, heating until 200°C and 24 h. Then, the biosorbent was activated in an over at 450°C for 10 min with oxidizing atmosphere.

2.4. Batch biosorption

The applicability of the low-cost adsorbent in water treatment process was tested in the biosorption of the chloroquine (CQ) from synthetic contaminant water in batch biosorption. The biosorption experiments were carried out in an orbital shaker (Tecnal TE-4200) at 135 rpm. Briefly, 20 mg of biosorbent HC-T and 20 mL of CQ solution (100 mg·L^{-1}) was placed inside a sealed Erlenmeyer flask and agitated for 24 h at 25°C, 35°C and 45°C. The biosorbent mass and CQ-solution volume were selected from previous tests in order to provide the maximum contaminant removal (in percentage). Samples were collected at different times and filtered in a 0.45 μm cellulose membrane. The residual CQ concentration in the samples were detected in a UV-Vis spectrophotometer (Hasch DR 5000) at 343 nm [19]. All experiments were performed in duplicates and the results were presented as average ± standard deviation. The HC-T biosorption capacity (q_e, mg·g^{-1}) was calculated according to Eq. (1).

$$q_e = \frac{V \cdot (C_i - C_e)}{m} \tag{1}$$

where C_i and C_e are the initial and equilibrium CQ concentrations, respectively (mg·L^{-1}); V is the volume of CQ working solution used (L); and m is the mass of HC-T used (g).

The effect of the pH of the chloroquine solution on the HC-T biosorption capacity was determined since it is an important parameter for the biosorption process and adsorbent efficiency [22]. For this purpose, the pH solution was adjusted to 2, 5, 7, 9 or 12 adding HCl (0.1 mol·L^{-1}) or NaOH (0.1 mol·L^{-1}) solutions dropwise. The same protocol for batch biosorption was used herein.

The kinetic and equilibrium biosorption experiments were conducted at the natural CQ solutions' pH (~6.0) since the changing of the pH in a water treatment plant is costly due to chemical consumption and may cause salinity problems. Pseudo-first-order, pseudo-second-order kinetic models as well as Elovich model were adjusted to the experimental data. The best model fit was determined by means of the determination coefficient (R^2) and square-root mean error (SRME). The biosorption equilibrium isotherms were obtained at 25°C, 35°C and 45°C using 20 mg of biosorbent at constant agitation (135 rpm) for 24 h. The initial CQ concentration (20 mL) varied from 20 to 120 mg·L^{-1} with pH ~ 6.0. The Langmuir, Freundlich and Sips isotherm models were fitted to the experimental equilibrium data. The best model fit was determined by means of the R^2 and SRME.

The thermodynamic analysis of the batch biosorption process was performed in order to determine the Gibb's free energy [$\Delta G°$; Eq. (2)], enthalpy [$\Delta H°$; Eq. (3)] and entropy [$\Delta S°$; Eq. (3)].

$$\Delta G° = -RT \ln K_c \tag{2}$$

$$\ln K_c = -\frac{\Delta H°}{RT} + \frac{\Delta S°}{R} \tag{3}$$

where R is the universal constant of gases (8.314 J·mol^{-1}·K^{-1}), T is the absolute temperature (K) and K_c is the equilibrium biosorption constant. For each temperature, the value of K_c was obtained by the extrapolation of the curve $L_n(q_e C^{-1}_e) \times q_e$ in the limit of $q_e \to 0$.

3. Results and discussion

3.1. Characterizations of SB and HC-T

The specific surface area (S_{BET}) for the HC-T was 187.80 m^2·g^{-1}, a significant increase from the original 16.86 m^2·g^{-1} in the SB process. An increase in the S_{BET} can be correlated to a higher biosorption capacity [14]. The basicity of the high-pressure boiler effluent that is in contact with the adsorbent during the hydrothermal process ends up corroding, when heated, the carbon-rich parts of the material structure leading to a secondary porosity and increasing the specific surface area. The obtained S_{BET} value is in agreement with reported values for sugarcane biomass such as the 131 m^2·g^{-1} for a biochar produced from sugarcane bagasse modified in a muffle at 450°C for 15 min only [23]. Jais et al. [24], reported a specific surface are of 8.10 m^2·g^{-1} for the sugarcane bagasse modified via hydrothermal process and when activated with NaOH, the area increased 3.4 times (27.55 m^2·g^{-1}). Mohamed et al. [25] reported a much lower area of 6.17 m^2·g^{-1} for a polyethyleneimine-modified sugarcane bagasse. The authors did not employ hydrothermal treatment to their adsorbent and the polymer coated the material surface, thus leading to the low S_{BET} reported. It is important to note that the HC-T reported herein was obtained using SB as obtained from the industry, that is, without any chemical or physical pretreatment, thus promoting its economic viability and potential biosorption capacity. Table 2 displays the carbon content and N$_2$-physisorption results for the HC-T.

As seen in Table 2, the average pore diameter of the HC-T biosorbent was 1.79 nm and total volume of pores of 1.51 cm^3·g^{-1} of which 0.08 cm^3·g^{-1} were due to micropores. The porosity of the microstructure was due to the presence of NaOH in the boiler water used in the HC-T process. The high-temperature of the HC-T process and the alkalinity of the BD effluent caused the micropores deconstructions [26,27] shown in the following reaction Eq. (4):

$$6NaOH + 2C \to 3Na_2O + CO \uparrow + CO_2 \uparrow + 3H_2 \uparrow \qquad (4)$$
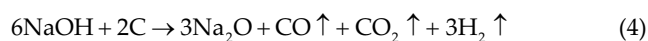
Even though the carbon was oxidated by the NaOH, the carbon content increased from ~38% to ~60% in the HC-T biosorbent, the high pH dissolved the unburnt biomass thus increasing the carbon content [27].

The SEM images for SB and HC-T (Fig. 1) were analyzed and corroborated the modifications in surface morphology and properties. For the SB (Fig. 1A), the micrography displayed the fibrous biomass, of irregular shape and roughness, common for sugarcane bagasse [28]. In contrast, the HC-T biosorbent surface morphology (Fig. 1B) showed the presence of small structures in its surface, possible originated from the chain-breaking from hemicellulose and pectin molecules due to HC process conditions [15,16]. The SB surface was clean and a small crack can be seen at the top-left corner of the HC-T biosorbent possibly due to the rapidly water vaporization or from the milling in the pretreatment step.

The thermogravimetric analysis/differential thermogravimetric analysis (TGA/DTG) technique was used to analyze the mass variation during the HC-T process due to thermal degradation and the results are illustrated in Fig. 2.

The mass loss seen in Fig. 2 is a function of the temperature, hydrothermal process conditions and the treatment performed in the samples [24]. The HC-T showed a significant decrease in mass starting at ~403°C. Since the HC-T process was carried out at 450°C for 10 min for carbon activation, it was expected that the biosorbent only showed mass loss for higher temperatures since at lower values the material already lost water and volatile compounds [19] such as the , approximately, 3.5% mass loss at <100°C and

Table 2
Carbon content and N$_2$-physisorption results for HC-T

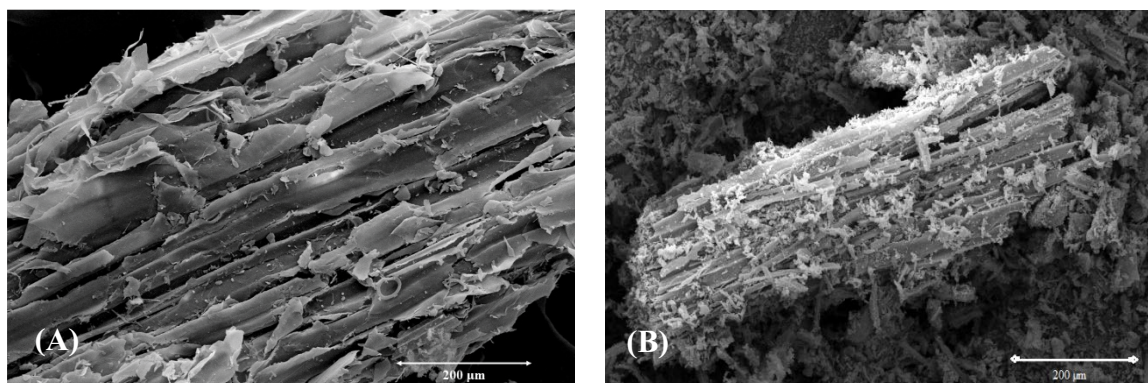| Property	HC-T
Specific surface area (m^2·g^{-1})	187.80
Average pore diameter (nm)	1.79
Total volume of pores (cm^3·g^{-1})	1.51
Volume of micropores (cm^3·g^{-1})	0.08
Carbon content (%)	60.11

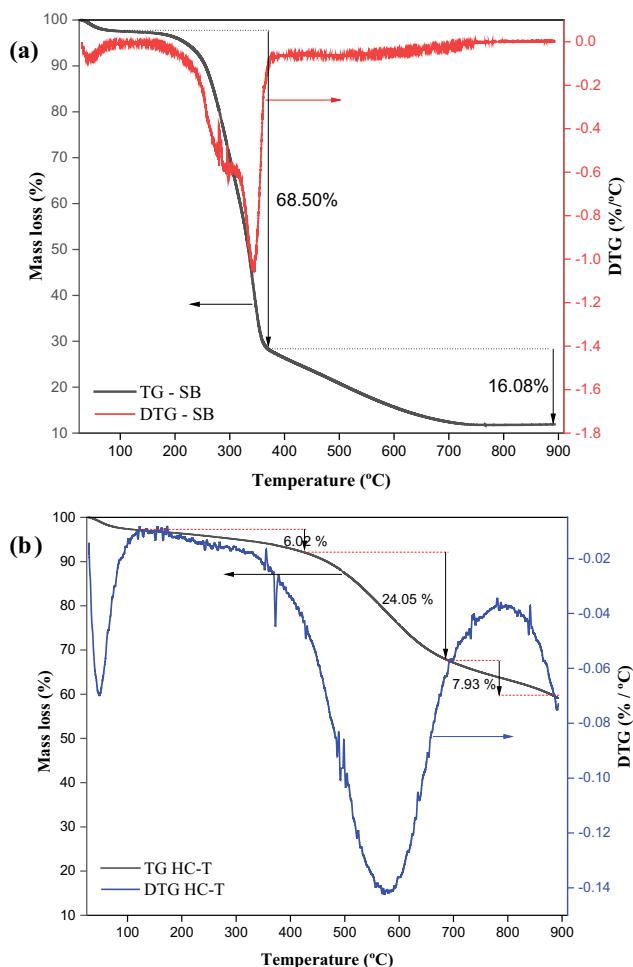Fig. 1. Scanning electron microscopy images of sugarcane bagasse (A) and HC-T (B).

Fig. 2. Thermogravimetric analysis/differential thermogravimetric analysis results for sugarcane bagasse (A) and HC-T biosorbent (B).

Fig. 3. Fourier-transform infrared spectrogram for sugarcane bagasse and HC-T.

~68.5% at <365°C seen in the nonhydrothermal-modified SB (Fig. 2A) [29].

The TGA result for HC-T (Fig. 2B) can be divided into three parts. In the first 6.02%, the mass loss was attributed to the thermal degradation of cellulose, hemicellulose and the initial lignin decomposition [30]. This trend was corroborated by the DTG curve where the first peak was attributed to the water evaporation and volatiles degradation, the second peak to the degradation of hemi- and cellulose and the third peak to the more thermally resistant lignin [29].

FT-IR technique is commonly applied to identify changes in the chemical structure in materials surfaces [30]. In this sense, the FT-IR results are displayed in Fig. 3 and the major chemical groups in the SB and HC-T surfaces were signaled and analyzed.

The analysis of Fig. 3 revealed the dominance of some chemical groups in the surface of both SB and HC-T adsorbent due to the intensity of the infrared spectra peaks. The lignocellulosic nature of sugarcane bagasse is associated to the presence of hydroxyl groups (3,420–3,396 cm^{-1}), thus the peak found at 3,440 cm^{-1} was attributed to the OH– associated with vibrations and axial deformations [31]. The peak
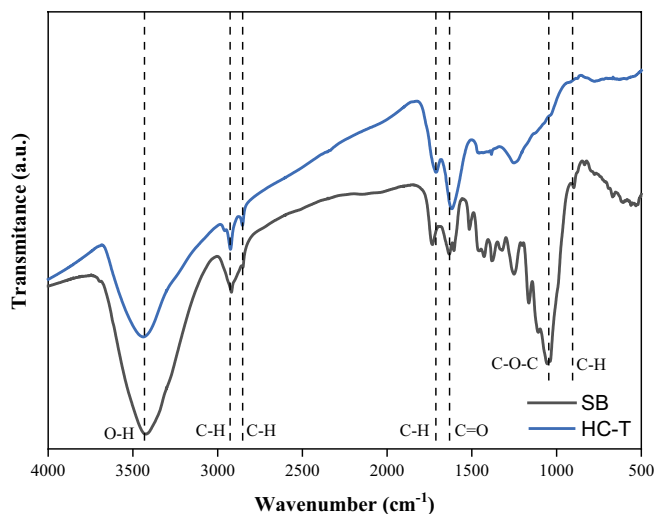
observed at 2,929 cm^{-1} was attributed to the C–H stretching from lignin and the peak at 2,857 cm^{-1} also from the C–H stretching but from aldehydes [32]. The peaks intensities found at 1,620–1,722 cm^{-1} are due to the aromatic ring (σ and π carbon bons and =O stretching vibration) [33]. The peak at 1,252 cm^{-1} was due to the vibrations of hydroxyl functional group [31] and near 1,100 cm^{-1} to the C–O–C bond vibration. To complement the FT-IR assay, XRD and Raman analysis were performed.

The XRD diffractogram for HC-T biosorbent and its Raman spectra are shown in Fig. 4.

As seen in Fig. 4A, the XRD for the low-cost adsorbent revealed a broad valley in the range of 10° and 25° 2θ associated with the amorphous structure of the carbon material, but the peak at ~20° due to cellulose was not found in the HC-T as it was thermally degraded during the process [34]. The increase in XRD intensity at ~27° is due to the presence of water [35]. In addition, the peak observed at 43.7 angle is due to the graphitic plane (100) [36].

In the Raman spectra of Fig. 4B two band intensities were found. The band at 1,360 cm^{-1} is called disorder-induced D-band and is attribute to structural defects, that is, disorders and to amorphous carbon, that is, sp^3 hybridized carbons [36]. The second band at 1,582 cm^{-1} is a graphitic G-band due to the in-plane vibrations from the sp^2 hybridized carbons [37]. It is of interest to characterize activated carbon materials by its level of graphitization through the area ratios of D- and G-bands (I_D/I_G), thus being a measure of disorderness in the carbon structure [38]. In the HC-T biosorbent, the calculated I_D/I_G ratio was 0.85, thus suggesting that the HC treatment did not increase the level of disorderness [12].

Another important characterization parameter for biosorbent materials used in water treatment processes is the pH of the point of zero charge (pH$_{PZC}$). When the pH of the contaminated solution is lower than the pH$_{PZC}$ the adsorbent remains protonated with a net positive charge and, therefore, the biosorption of anionic molecules is favorable through mutual attraction. However, for a pH greater than the pH$_{PZC}$, then the biosorption site would pose a net negative
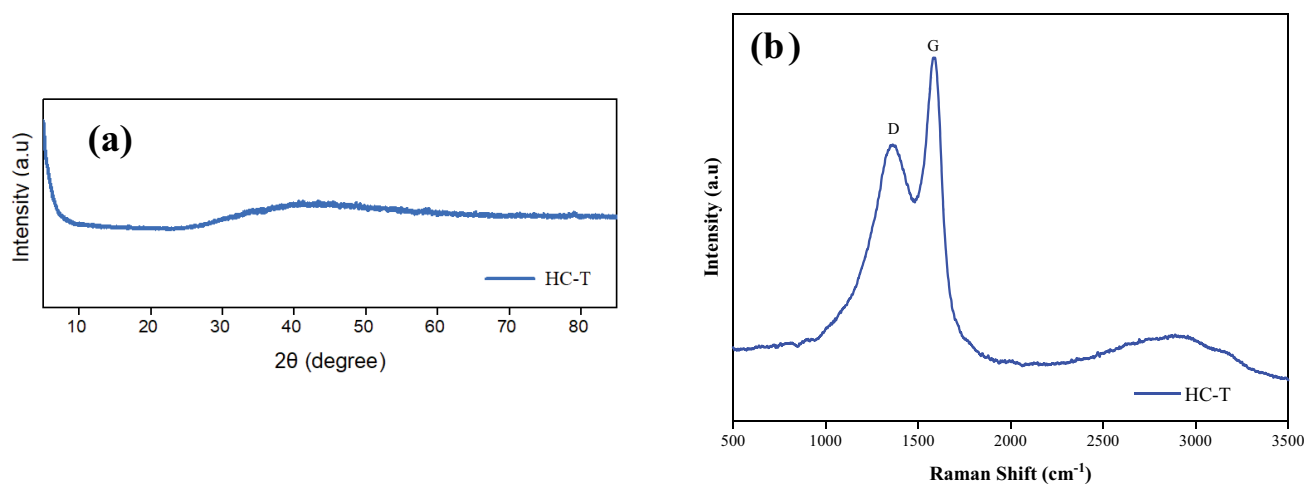
Fig. 4. X-ray diffractograms for HC-T biosorbent (A) and Raman spectra (B).

charge due to the adsorbent deprotonation, thus enhancing the biosorption of cationic contaminants [39]. For the HC-T biosorbent, the pH_{PZC} is shown in Fig. 5.

As discussed, the pH_{PZC} can be a critical factor in the selection of sorbent materials as it can hinder or not the biosorption efficiency due to adsorbent-contaminant interaction [19]. The analysis of Fig. 5 revealed that the HC-T biosorbent poses an acid pH_{PZC} of 3.46. This value can be correlated to the presence of carboxylic acids in the biosorbent biomass origin [40]. Therefore, $pH > pH_{PZC}$ suggests that the HC-T adsorbent has a negative net charge and that the biosorption of cationic molecules are favorable [41].

3.2. Batch biosorption results

The effect of the pH of the chloroquine-contaminated solution was analyzed and the results are shown in Fig. 6, expressed in terms of the HC-T biosorption capacity.

Fig. 6 reveals that an increase in the pH of the CQ-contaminated solution from 2 up to 12 was followed by an increase in the HC-T biosorption capacity (from ~75 to ~93 mg·g^{-1}). An increase in basicity implies in an excess of OH$^-$ in the liquid phase and a net negative charge at the HC-T surface. Therefore, basic conditions enhanced the biosorption of cationic molecules such as chloroquine [19]. Similar performance is reported with natural and treated sugarcane bagasse in the biosorption of methylene blue [42]. But the opposite trend is reported for the biosorption of phosphate ions with a chitosan-modified sugarcane bagasse [32], that is, an increase in the solution pH lowered the biosorption capacity until a minimum at pH = 10 which was attributed to the deprotonation of amino functional groups [32].

However, the kinetic and equilibrium biosorption experiments were conducted at pH~6,0 which is the natural CQ solutions' pH. This is due to the operational problems originated from changing the pH in a water treatment plant which is costly due to chemical consumption and may cause salinity problems, thus reducing the water quality.

The kinetic biosorption of chloroquine on the HC-T hydrochar is shown in Fig 7 alongside with the fitting of pseudo-first-order and pseudo-second-order kinetic models.
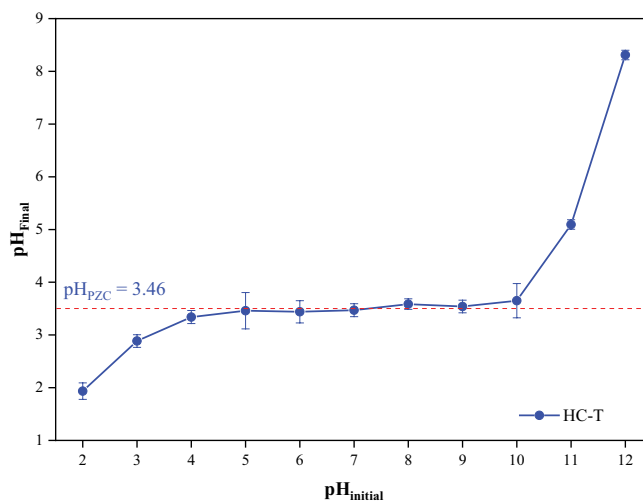

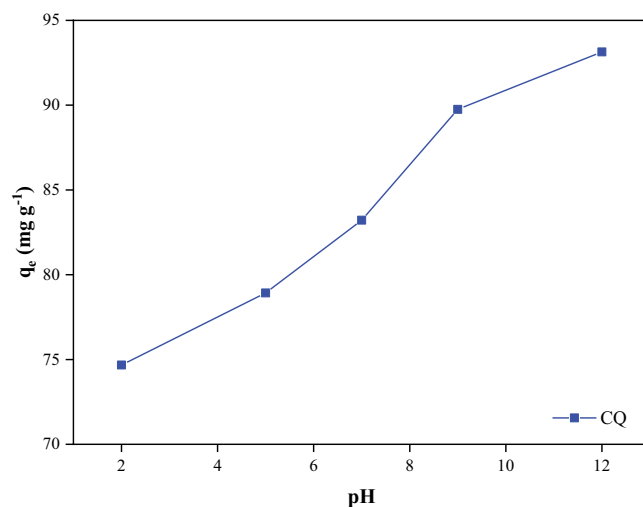Fig. 5. pH_{PZC} obtained for HC-T biosorbent.

Fig. 6. Effect of pH in the biosorption of CQ. Conditions: 20 mg of HC-T, 20 mL of $[CQ]_0$ = 100 mg·L^{-1}, 135 rpm, t = 24 h and T = 30°C.
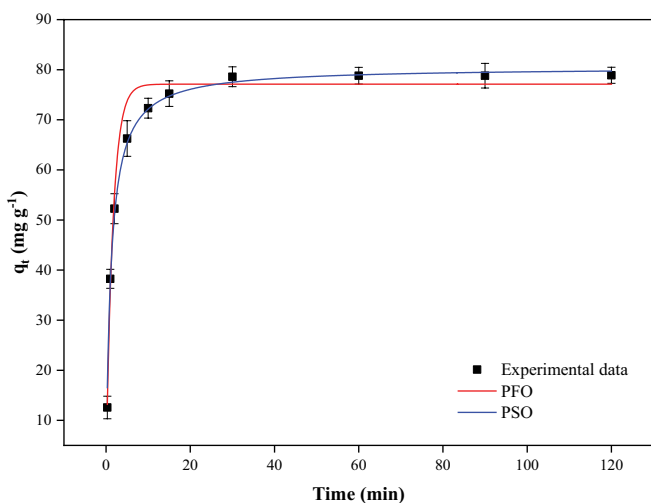
Fig. 7. Experimental results and model fitting for the kinetic biosorption of CQ HC-T as adsorbent. Conditions: 20 mg of HC-T, 20 mL of $[CQ]_0 = 100$ mg·L^{-1}, 135 rpm, pH = 6.0 and T = 30°C.

Table 3
Kinetic model fitting parameters and statistics for CQ biosorption with HC-T

Parameter	Value
Pseudo-first-order	
$q_{e,cal}$ (mg·g^{-1})	77.112 ± 1.122
k_1 (min^{-1})	0.625 ± 0.052
R^2	0.983
SRME	2.029
Pseudo-second-order	
$q_{e,cal}$ (mg·g^{-1})	80.501 ± 0.666
k_2 (g·mg^{-1}·min^{-1})	0.010 ± 1.659
R^2	0.995
SRME	0.542

$q_{e,cal}$: biosorption capacity at equilibrium calculated (mg·g^{-1}); k_1: pseudo-first-order model rate constant (min^{-1}); k_2: pseudo-second-order model rate constant (g·mg^{-1}·min^{-1}).

The results showed a rapid biosorption rate in the initial 10 min followed by a slow biosorption rate due to less availability of biosorption sites, thus reaching the dynamic equilibrium conditions after ~60 min meaning that the biosorption and desorption velocities of CQ are equal.

The biosorption of CQ over a graphene oxide-agar composite revealed a similar process with a rapid biosorption rate at initial times followed by equilibrium conditions after ~50 min for various working solution concentrations (5–20 mg·L^{-1}) [19]. Longer periods of time was obtained by [43] with acid-activated *Hibiscus sabdariffa* seed pods (*t* > 240 min). However, the authors used an acid solution for CQ biosorption (pH = 3.0) and they demonstrated that the removal efficiency was over 90% for that condition. It is important to remember that CQ admits three pKa values (4.0, 8.5 and 10.2) that allows an efficient biosorption over a wide range of pH [44]. Therefore, the optimum pH for CQ biosorption would be different according to the adsorbent surface functional groups and charge distribution [43].

According to the statistical values of the kinetic models fitting (Table 3), the pseudo-second-order model with $R^2 = 0.995$ and SRME = 0.542 was the best fit. For the pseudo-second-order model the biosorption capacity at equilibrium conditions ($q_{e,cal}$) was ~80.5 mg·g^{-1} with a pseudo-second-order rate constant (k_2) of 0.010 g·mg^{-1}·min^{-1}. It is worth to note that the standard deviation calculated for k_2 was high, but the pseudo-second-order model was still considered the best model fit due to statistical parameters and, in addition, the fact that the $q_{e,cal}$ was close to the experimental value ($q_{e,exp}$ = 78.8 mg·g^{-1}, an error lesser than 5%).

In order to understand the step-dominant mechanism and the rate-limiting-step for the CQ biosorption on HC-T, the Weber–Morris intraparticle diffusion model [45] was used and the results are shown in Fig. 8.

According to Fig. 8, the biosorption process is divided in three stages in which different biosorption rates and conditions are applied: the stage I indicates the liquid-film diffusion, state II indicates the intraparticle diffusion and stage
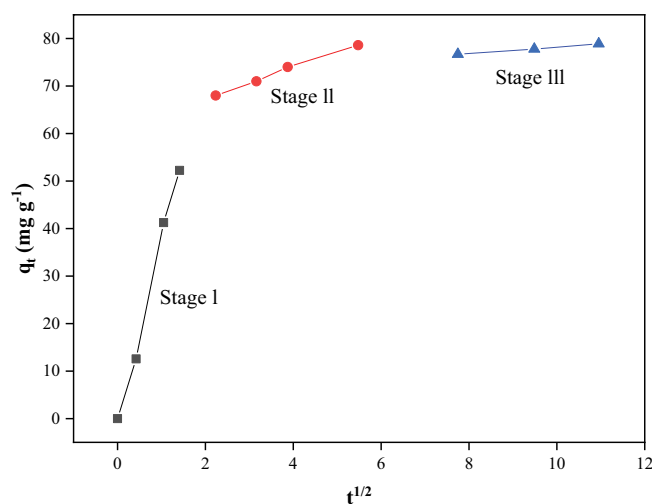

Fig. 8. Intraparticle diffusion mechanism for CQ using HC-T as adsorbent.

III is the equilibrium [45]. The fitted Weber–Morris model parameters for each stage are shown in Table 4.

Since the graph for stage I intercepts its origin point, the liquid-film diffusion is the limiting-step in the CQ biosorption on HC-T biosorbent, evidenced by the increase in constant *C* value on the subsequent stages, that is, an increase in the boundary thickness [19]. An intraparticle diffusion-limited biosorption was obtained by [46] using a Fe_3O_4-functionalized agro-industrial residue for CQ biosorption [43] also reported a diffusion-limited process. Aiming an industrial perspective for water treatment process, the liquid-film limiting biosorption is preferable since biosorption parameters can be controlled through fluid dynamics as, for example, in a continuous biosorption column.

The experimental data for the biosorption isotherm experiments are shown in Fig. 9, which illustrates the

biosorption capacity (q_e) for the HC-T hydrochar for different equilibrium concentrations of CQ (C_e) at constant temperature. The results showed that an increase in temperature was followed by an increase in the HC-T biosorption

Table 4
Intraparticle diffusion model fitting parameters for CQ biosorption on HC-T

Parameters	Stage I	Stage II	Stage III
C (mg·g^{-1}·h$^{-0.5}$)	1.203	60.759	71.411
K_{id} (mg·g^{-1})	38.408	3.295	0.679
R^2	0.992	0.994	0.998

K_{id} is the intraparticle diffusion rate constant (mg·g^{-1}·min$^{-0.5}$), calculated by the slope of the linear graph of q_t vs. $t^{0.5}$ for each stage and C is the constant related to the boundary layer thickness (intercept of the linear graph).

capacity, reaching a maximum experimental biosorption of CQ of ~74 mg·g^{-1} at 45°C.

The Langmuir, Freundlich and Sips isotherm models were fitted to the experimental data (Fig. 9) and the best fitted model, according to statistical parameters shown in Table 5, was the Sips model with $R^2 > 0.9$ for all temperatures analyzed. For the Sips isotherm model, the maximum biosorption capacity (q_m) increased from 74 to 135 mg·g^{-1} and the Sips model constant (K_S) increased from 0.353 to 0.882 mL·mg^{-1} with increasing temperature from 25°C to 45°C.

The exponential factor (n) in the Sips model decreased from 2.586 to 1.545 when temperature increased from 25°C to 35°C, but increased to 2.651 when the working solution was constant at 45°C. One can infer, from the following discussion, that the increase in the exponential factor n from 25°C to 45°C can be related to the increase in the maximum biosorption capacity since more CQ molecules can interact with the same vacancy.
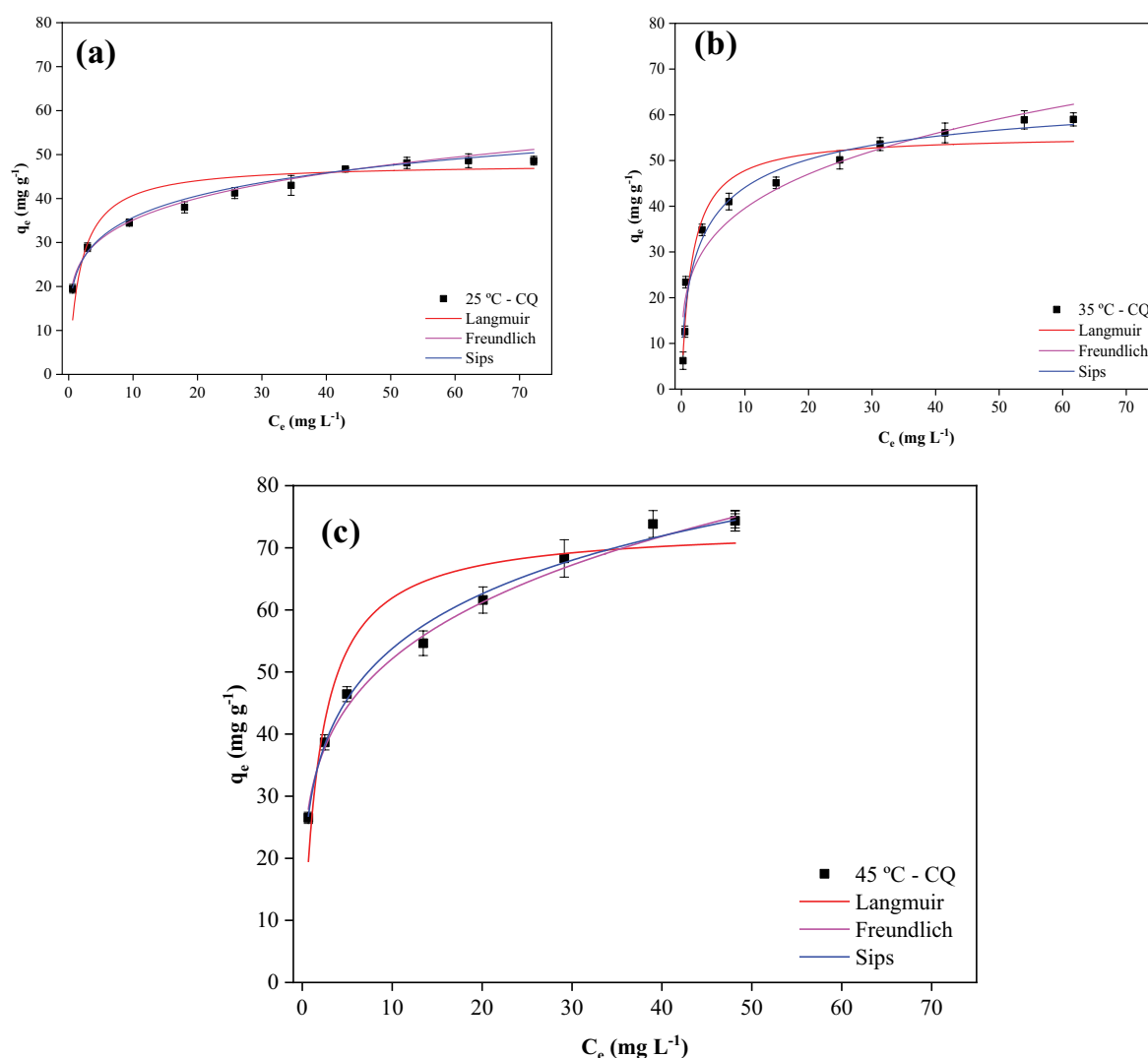

Fig. 9. Biosorption isotherms for CQ with adsorbent HC-T. Conditions: HC-T 20 mg, pH = 6.0, [CQ]$_0$ from 20 to 120 mg·L^{-1}, t = 24 h, 135 rpm and T = 25°C (A), 35°C (B) and 45°C (C).

Table 5
Statistics and isotherms model fitting parameter for the biosorption of CQ using HC-T

Langmuir	25°C	35°C	45°C
q_m (mg·g^{-1})	48.006 ± 1.312	55.584 ± 2.314	73.449 ± 2.342
K_L (L·mg^{-1})	0.557 ± 0.164	0.613 ± 0.132	0.634 ± 0.118
R^2	0.874	0.944	0.915
SRME	18.006	8.936	17.333
Freundlich	25°C	35°C	45°C
K_F (mg·g^{-1}(mg·L^{-1})$^{-1/nF}$)	22.643 ± 0.797	22.763 ± 1.992	23.591 ± 0.665
n	5.249 ± 0.266	4.005 ± 0.436	3.320 ± 0.123
R^2	0.987	0.937	0.995
SRME	1.731	10.040	1.065
Sips	25°C	35°C	45°C
q_m (mg·g^{-1})	74.137 ± 25.402	77.073 ± 17.512	135.394 ± 15.001
K_S (mL·mg^{-1})	0.353 ± 0.104	0.476 ± 0.121	0.882 ± 0.038
n	2.586 ± 0.990	1.545 ± 0.299	2.651 ± 0.195
R^2	0.999	0.973	0.998
SRME	0.883	1.255	0.288

The Sips isotherm is a combination of the Langmuir and Freundlich isotherms and is commonly referred to as the Langmuir–Freundlich isotherm [47]. Its distinction from the Langmuir isotherm is the fact that the Sips isotherm considers that n molecules, in this case CQ, can be adsorbed in just one biosorption site on the HC-T adsorbent and this process is represented by Eq. (5).

$$n\text{CQ}_{\text{liquid phase}} + \text{HC} - \text{T}_{\text{vacancy}} \rightleftharpoons \text{HC} - \text{T}_{n\text{CQ ads}} \tag{5}$$
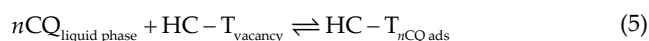
At equilibrium conditions, the equilibrium constant (considering the Sips model nomenclature applied for CQ biosorption on HC-T) is set as Eq. (6).

$$K_S = \frac{\left[\text{HC} - \text{T}_{n\text{CQ ads}}\right]}{\left[\text{CQ}_{\text{liquid phase}}\right]^n \left[\text{HC} - \text{T}_{\text{vacancy}}\right]} \tag{6}$$

Since the total number of biosorption-sites is constant, a balance between the vacancy and the CQ-occupied biosorption sites can be represented as follows:

$$\text{HC} - \text{T}_{\text{available}} = \text{HC} - \text{T}_{\text{vacancy}} + \text{HC} - \text{T}_{n\text{CQ ads}} \tag{7}$$

However, the fact that n molecules of chloroquine can be adsorbed in one biosorption site on the surface of the adsorbent introduces the exponential factor in the Sips isotherm model equation, thus resembling the Freundlich model. Then, the substitution of Eq. (7) in Eq. (6) follows the Sips isotherm model according to Eq. (8).

$$\left[\text{HC} - \text{T}_{n\text{CQ ads}}\right] = \frac{K_S\left[\text{HC} - \text{T}_{\text{available}}\right]\left[\text{CQ}_{\text{liquid phase}}\right]^n}{1 + K_S\left[\text{CQ}_{\text{liquid phase}}\right]^n} \tag{8}$$

in which [HC − $T_{n\text{CQ ads}}$] represents the equilibrium concentration of *n* molecules of CQ adsorbed in the HC-T

Table 6
Calculated parameters of the biosorption thermodynamic equation for the biosorption of CQ using HC-T as adsorbent

T (K)	$\Delta G°$ (kJ·mol^{-1})	$\Delta H°$ (kJ·mol^{-1})	$\Delta S°$ (kJ·mol^{-1}·K^{-1})
298	−29.791		
308	−31.962	35.961	0.217
318	−34.135		

biosorbent, [HC − $T_{\text{available}}$] represents the maximum biosorption capacity of HC-T biosorbent and [CQ$_{\text{liquid phase}}$] is the equilibrium concentration of CQ in the working solution.

Eq. (8) is commonly written as Eq. (9) [47].

$$q_e = \frac{K_S q_m C_e^n}{1 + K_S C_e^n} \tag{9}$$

From this discussion and the fact that the isotherms obtained (Fig. 9) are classified as L-2 according to Giles classification meaning that there is an energy barrier before additional adsorption can occur [48], one can explain the increase in the exponential factor n from 25°C to 45°C.

The thermodynamic parameters of enthalpy ($\Delta H°$) and entropy ($\Delta S°$) were estimated from the slope and intercept of linear plot $\ln K_c$ with $1/T$ and the Gibbs energy ($\Delta G°$) was calculated using Eq. (2) and the data are shown in Table 6. For all studied temperatures the value of $\Delta G°$ was negative, meaning that CQ molecules are spontaneously confined at the HC-T surface. The positive value of $\Delta H°$ corroborates that the biosorption of CQ is an endothermic process and the positive value of $\Delta S°$ indicates an increase in the randomness of solid–liquid interactions [49].

4. Conclusion

The presence of pharmaceutical drugs such as chloroquine in superficial and groundwaters is of growing

concerns and this problem needs a solution. In this sense, this work synthesized a low-cost biosorbent, using sugarcane bagasse and high-pressure boiler discharge effluent, for chloroquine biosorption from synthetic contaminated water. The biosorbent characterization revealed a higher specific surface area (187.80 m^2·g^{-1}) than the *in natura* sugarcane bagasse and a pH$_{PZC}$ of 3.46 indicating that the adsorbent is negatively charged, thus suggesting electrostatic interaction with the positive functional groups of chloroquine. The pseudo-second-order kinetic and Sips isotherm models were the best fitted to experimental data. The thermodynamic parameters indicated an endothermic and spontaneous biosorption. The maximum biosorption capacity reported is 78.34 mg (63.69%) of chloroquine per unit mass of low-cost biosorbent at 45°C. In conclusion, HC-T is a promising biosorbent, synthesized with an ecofriendly process, for the removal of chloroquine from contaminated waters due to the great availability, quantity and low-cost of sugarcane bagasse in the Brazilian territory, allied with the reusability of high-pressure boiler water. It is important to emphasize that the competitivity of a sugar-alcohol industry is increased when residues, solid and/or effluents, are reutilized or poses a noble destination, thus gaining financial leverage due to lesser operational costs and the industrial process is intensified towards a circular economy and the environmental, social and corporate governance (ESG) goals.

Data availability statement

All data included in this study are available upon request by contact with the corresponding author.

Acknowledgements

References

[1] L. Zou, L. Dai, X. Zhang, Z. Zhang, Z. Zhang, Hydroxychloroquine and chloroquine: a potential and controversial treatment for COVID-19, Arch. Pharm. Res., 43 (2020) 765–772.

[2] M.M. Melo, M.R.F. Costa, F.S.S. Filho, J.D. Brito-Sousa, A.C.G. Almeida, W.M. Monteiro, G.C. Melo, J.L.F. Vieira, M.G.C. Alecrim, Pharmacokinetics of chloroquine in patients with malaria by *P. vivax* from the Western Brazilian Amazon basin, Biomed. Pharm., 149 (2022) 112874, doi: 10.1016/j.biopha.2022.112874.

[3] S.H. Joo, H. Choi, Field grand challenge with emerging superbugs and the novel coronavirus (SARS-CoV-2) on plastics and in water, J. Environ. Chem. Eng., 9 (2021) 104721, doi: 10.1016/j.jece.2020.104721.

[4] P.E. Rosenfeld, L.G.H. Feng, In: 16-Emerging Contaminants, Risks of Hazardous Wastes, Elseveir, 2011, pp. 215–222. Available at: http://dx.doi.org/10.1016/B978-1-4377-7842-7.00016-7

[5] S. Rollemberg, A.N. de Barros, J.P.M. de Lima, Avaliação da contaminação, sobrevivência e remoção do coronavírus em sistemas de tratamento de esgoto sanitário, Rev. Tecnol., 41 (2020) 1–15.

[6] J. Hu, N. Hellgeth, C. Cabay, J. Cark, F.J. Oliaro, W.V. Bonn, E.M. Hartmann, Towards understanding microbial degradation of chloroquine in large saltwater systems, Sci. Total Environ., 807 (2022) 150532, doi: 10.1016/j.scitotenv.2021.150532.

[7] J. Liu, Y. Hu, X. Li, C. Xiao, Y. Shi, Y. Chen, J. Cheng, X. Zhu, G. Wang, J. Xie, High-efficient degradation of chloroquine phosphate by oxygen doping MoS$_2$ co-catalytic Fenton reaction, J. Hazard. Mater., 458 (2023) 131894, doi: 10.1016/j.jhazmat.2023.131894.

[8] S. Midassi, A. Bedoui, N. Bensalah, Efficient degradation of chloroquine drug by electro-Fenton oxidation: effects of operating conditions and degradation mechanism, Chemosphere, 260 (2020) 127558, doi: 10.1016/j.chemosphere.2020.127558.

[9] M. Lindroos, D. Hörnström, G. Larsson, M. Gustavsson, A.J.A. van Maris, Continuous removal of the model pharmaceutical chloroquine from water using melanin-covered *Escherichia coli* in a membrane bioreactor, J. Hazard. Mater., 365 (2019) 74–80.

[10] D. Dabić, S. Dabić, I. Škorić, The role of photodegradation in the environmental fate of hydroxychloroquine, Chemosphere, 230 (2019) 268–277.

[11] I. Ushiki, M. Tashiro, R.L. Smith Jr., Measurement and modeling of adsorption equilibria of imidazolium-based ionic liquids on activated carbon from aqueoussolutions, Fluid Phase Equilib., 441 (2017) 17–23.

[12] H.H.C. Lima, R.S. Maniezzo, V.L. Kupfer, M.R. Guilherme, M.P. Moises, P.A. Arroyo, A.W. Rinaldi, Hydrochars based on cigarette butts as a recycled material for the adsorption of pollutants, J. Environ. Chem. Eng., 6 (2018) 7054–7061.

[13] S. Praveen, J. Jegan, T.B. Pushpa, R. Gokulan, L. Bulgariu, Biochar for removal of dyes in contaminated water: an overwiew, Biochar, 4 (2022) 1–16, doi: 10.1007/s42773-022-00131-8.

[14] C.H. Maeda, A.L. Moretti, A. Diório, M.U.C. Braga, F.B. Scheufele, M.A.S.D. Barros, P.A. Arroyo, The influence of electrolytes in the adsorption kinetics of reactive BF-5G blue dye on bone char: a mass transfer model, Environ. Technol., (2022) 1–17, doi: 10.1080/09593330.2022.2128891.

[15] F.L. Seixas, M.L. Gimenes, N.R.C. Fernandes-Machado, Treatment of vinasse by adsorption on carbon from sugar cane bagasse, Quim. Nova, 39 (2016) 172–179.

[16] A. Moubarik, N. Grimi, Valorization of olive stone and sugarcane bagasse by-products as biosorbbents for the removal of cadmium from aqueous solution, Food Res. Int., 73 (2015) 169–175.

[17] CONAB (National Company of Supplying), "Safra 2022/23", BOLETIM DA SAFRA DE CANA-DE-AÇÚCAR, 2022. Available at: https://www.conab.gov.br/info-agro/safras/cana/boletim-da-safra-de-cana-de-acucar (Accessed Jul. 10, 2022).

[18] D. Mantovani, H.B. Quesada, R.S. Antônio, L.F. Cusioli, L. Nishi, A. Diório, P.F. Soares, R. Bergamasco, M.F. Vieira, Adsorption of methylene blue from effluent using golden mussel (*Limnoperna fostunei*) shell as a low-cost material, Desal. Water Treat., 188 (2020) 232–238.

[19] C.M.B. de Araujo, G. Wernke, M.G. Ghislandi, A. Diório, M.F. Vieira, R. Bergamasco, M.A.M. Sobrinho, A.E. Rodrigues, Continuous removal of pharmaceutical drug chloroquine and safranin-O dye from water using agar-graphene oxide hydrogel: selective adsorption in batch and fixed-bed experiments, Environ. Res., 216 (2023) 114425, doi: 10.1016/j.envres.2022.114425.

[20] S. Brunauer, P.H. Emmett, E. Teller, Adsorption of gases in multimolecular layers, J. Am. Chem. Soc., 60 (1938) 309–319.

[21] J.R. Regalbuto, J.O. Robles, The Engineering of Pt/Carbon Catalyst Preparation, Univ. Illinois, Chicago, 2004, 13 p.

[22] A. Bonilla-Petriciolet, D.I. Mendoza-Castillo, H.E. Reynel-Ávila, Adsorption Process for Water Treatment and Purification, Aguascalientes, Springer, México, 2017.

[23] M.M. Jacob, M. Ponnuchamy, A. Kapoor, P. Sivaraman, Adsorptive decontamination of organophosphate pesticide chloropyrifos from aqueous systems using bagasse-derived biochar alginate beads: thermodynamic, equilibrium, and kinetic studies, Chem. Eng. Res. Des., 186 (2022) 241–251.

[24] F.M. Jais, C.Y. Chee, Z. Ismail, S. Ibrahim, Experimental design via NaOH actiation process and statistical analysis for activated sugarcane bagasse hydrochar for removal of

dye and antibiotic, J. Environ. Chem. Eng., 9 (2021) 104829, doi: 10.1016/j.jece.2020.104829.

[25] N.B. Mohamed, N. Ngadi, S. Wong, N.Y. Yahya, O. Hassan, I.M. Inuwa, L.A. Opotu, N. Ali, Facile synthesis of polyethylenimine-modified sugarcane bagasse adsorbent for removal of anionic dye in aqueous solution, Sci. Afr., 16 (2022) e01135, doi: 10.1016/j.sciaf.2022.e01135.

[26] A. Islam, M.J. Ahmed, W.A. Khanday, M. Asif, B.H. Hameed, Mesoporous activated coconut shell-derived hydrochar prepared via hydrothermal carbonization-NaOH activation for methylene blue adsorption, J. Environ. Manage., 203 (2017) 237–244.

[27] G. Prasannamedha, P.S. Kumar, R. Mehala, T.J. Sharumitha, D. Surendhar, Enhanced adsorptive removal of sulfa-methoxazole from water using biochar derived from hydro-thermal carbonization of sugarcane bagasse, J. Hazard. Mater., 407 (2021) 124825, doi: 10.1016/j.jhazmat.2020.124825.

[28] J.A. Oliveira, F.A. Cunha, L.A.M. Ruotolo, Synthesis of zeolite from sugarcane bagasse fly ash and its application as a low-cost adsorbent to remove heavy metals, J. Cleaner Prod., 229 (2019) 956–963.

[29] L. Bai, X. Su, J. Feng, S. Ma, Preparation of sugarcane bagasse biochar/nano-iron oxide composite and mechanism of its Cr(VI) adsorption in water, J. Cleaner Prod., 320 (2021) 128723, doi: 10.1016/j.jclepro.2021.128723.

[30] J. Hu, D. Shen, S. Wu, H. Zhang, R. Xiao, Effect of temperature on structure evolution in char from hydrothermal degradation of lignin, J. Anal. Appl. Pyrolysis, 106 (2014) 118–124.

[31] A.R. de Almeida, F.C. Monteiro, J.F.H.L. Monteiro, E.R.L. Tiburtius, C.A. Pessôa, Photocatalytic oxidation of textile dye using sugarcane bagasse-Nb$_2$O$_5$ as a catalyst, J. Photochem. Photobiol., A, 432 (2022) 114103, doi: 10.1016/j.jphotochem.2022.114103.

[32] A. Manyatshe, Z.E.D. Cele, M.O. Balogun, T.T.I. Nkambule, T.A.M. Msagati, Chitosan modified sugarcane bagasse biochar for the adsorption of inorganic phosphate ions from aqueous solution, J. Environ. Chem. Eng., 10 (2022) 108243, doi: 10.1016/j.jece.2022.108243.

[33] A.R. Gonçalves, E. Esposito, P. Benar, Evaluation of *Panus tigrinus* in the delignification of sugarcane bagasse by FTIR-PCA and pulp properties, J. Biotechnol., 66 (1998) 177–185.

[34] L. Cermakova, I. Kopecka, M. Pivokonsky, L. Pivokonska, V. Janda, Removal of cyanobacterial amino acids in water treatment by activated carbon adsorption, Sep. Purif. Technol., 173 (2017) 330–338.

[35] J.P. Farias, B.C. Okeke, F.D. de Ávila, C.F. Demarco, M.S. Silva, F.A.O. Camargo, F.M. Bento, S. Pieniz, R. Andreazza, Biotechnology process for microbial lipid synthesis from enzymatic hydrolysate of pre-treated sugarcane bagasse for potential bio-oil production, Renewable Energy, 205 (2023) 174–184.

[36] Mohit, N. Yadav, S.A. Hashmi, High energy density solid-state supercapacitors based on porous carbon electrodes derived from

pre-treated biowaste precursor sugarcane bagasse, J. Energy Storage, 55 (2022) 105421, doi: 10.1016/j.est.2022.105421.

[37] H.H.C. Lima, R.S. Maniezzo, M.E.G. Llop, V.L. Kupfer, P.A. Arroyo, M.R. Guilherme, A.F. Rubira, E.M. Girotto, A.W. Rinaldi, Synthesis and characterization of pecan nutshell-based adsorbent with high specific area and high methylene blue adsorption capacity, J. Mol. Liq., 276 (2019) 570–576.

[38] A.C. Ferrari, J. Robertson, Interpretation of Raman spectra of disordered and amorphous carbon, Phys. Rev., 31 (1969) 632–645.

[39] D. Ewis, M.M. Ba-Abbad, A. Benamor, M.H. El-Naas, Adsorption of organic water pollutants by clays and clay minerals composites: a comprehensive review, Appl. Clay Sci., 229 (2022) 106686, doi: 10.1016/j.clay.2022.106686.

[40] K. Zhang, H. Hu, L. Zhang, Q. Chen, Surface charge properties of red mud particles generated from Chinese diaspore bauxite, Trans. Nonferrous Met. Soc. China, 18 (2008) 1285–1289.

[41] D. Chvedov, S. Ostap, T. Le, Surface properties of red mud particles from potentiometric titration, Colloids Surf., A, 182 (2001) 131–141.

[42] K. Al-Mokhalelati, I. Al-Bakri, N. Al Shibeh Al Wattar, Adsorption of methylene blue onto sugarcane bagasse-based adsorbent materials, J. Phys. Org. Chem., 34 (2021) 1–9.

[43] D.T. Bankole, A.P. Oluyori, A.A. Inyinbor, Acid-activated *Hibiscus sabdariffa* seed pods biochar for the adsorption of chloroquine phosphate: prediction of adsorption efficiency via machine learning approach, S. Afr. J. Chem. Eng., 42 (2022) 162–175.

[44] R.L. Schroeder, J.P. Gerber, Chloroquine and hydroxychloro-quine binding to melanin: some possible consequences for pathologies, Toxicol. Rep., 1 (2014) 963–968.

[45] J.C. Weber, W.J., Morris, Kinetics of adsorption on carbon from solutions, J. Sanit. Eng. Div., 89 (1963) 31–60.

[46] T.B. Vidovix, E.F.D. Januário, R. Bergamasco, A.M.S. Vieira, Evaluation of agro-industrial residue functionalized with iron oxide magnetic nanoparticles for chloroquine removal from contaminated water, Mater. Lett., 326 (2022) 132915, doi: 10.1016/j.matlet.2022.132915.

[47] R. Sips, The structure of a catalyst surface, J. Chem. Phys., 16 (1948) 490–495.

[48] H. Straioto, P.V. Viotto, A.A. de Moura, A. Diório, M.H.N.O. Scaliante, W.M. Moreira, M.F. Vieira, R. Bergamasco, Modification of natural zeolite clinoptilolite and its application in the adsorption of herbicides, Environ. Technol., 1 (2022) 1–16, doi: 10.1080/09593330.2022.2077134.

[49] M. Pecchi, F. Patuzzi, V. Benedetti, R. Di, M. Baratieri, Thermodynamics of hydrothermal carbonization: assessment of the heat release profile and process enthalpy change, Fuel Process. Technol., 197 (2019) 106206, doi: 10.1016/j.fuproc.2019.106206.